

Aalborg Universitet



Frequency Stability of Hierarchically Controlled Hybrid Photovoltaic-Battery-Hydropower Microgrids

Guan, Yajuan; Quintero, Juan Carlos Vasquez; Guerrero, Josep M.; Wang, Yibo; Feng, Wei

Published in:
I E E Transactions on Industry Applications

DOI (link to publication from Publisher):
[10.1109/TIA.2015.2458954](https://doi.org/10.1109/TIA.2015.2458954)

Publication date:
2015

Document Version
Early version, also known as pre-print

[Link to publication from Aalborg University](#)

Citation for published version (APA):
Guan, Y., Quintero, J. C. V., Guerrero, J. M., Wang, Y., & Feng, W. (2015). Frequency Stability of Hierarchically Controlled Hybrid Photovoltaic-Battery-Hydropower Microgrids. *I E E Transactions on Industry Applications*, 51(6), 4729-4742. <https://doi.org/10.1109/TIA.2015.2458954>

General rights

Copyright and moral rights for the publications made accessible in the public portal are retained by the authors and/or other copyright owners and it is a condition of accessing publications that users recognise and abide by the legal requirements associated with these rights.

- Users may download and print one copy of any publication from the public portal for the purpose of private study or research.
- You may not further distribute the material or use it for any profit-making activity or commercial gain
- You may freely distribute the URL identifying the publication in the public portal -

Take down policy

If you believe that this document breaches copyright please contact us at vbn@aub.aau.dk providing details, and we will remove access to the work immediately and investigate your claim.

Frequency Stability of Hierarchically Controlled Hybrid Photovoltaic-Battery-Hydropower Microgrids

Yajuan Guan

Student Member, IEEE
Aalborg University
Pontoppidanstraede 101
Aalborg, 9220, Denmark
ygu@et.aau.dk

Juan C. Vasquez

Senior Member, IEEE
Aalborg University
Pontoppidanstraede 101
Aalborg, 9220, Denmark
juq@et.aau.dk

Josep M. Guerrero

Fellow, IEEE
Aalborg University
Pontoppidanstraede 101
Aalborg, 9220, Denmark
joz@et.aau.dk

Yibo Wang, Wei Feng

Institute of Electrical
Engineering
Chinese Academy of Sciences
Beijing, 100190, China
{wyb, fw}@mail.iee.ac.cn

Abstract -- Hybrid photovoltaic (PV) -battery-hydropower microgrids can be considered to enhance electricity accessibility and availability in remote areas. However, the coexistence of different renewable energy sources with different inertias and control strategies may affect system stability. In this paper, a hierarchical controller for hybrid PV-battery-hydropower microgrid is proposed in order to achieve the parallel operation of hydropower and PV-battery system with different rates, and to guarantee power sharing performance among PV voltage controlled inverters, while the required power to hydropower-based local grid is supplied. In this case, the PV-battery system will operate as a PQ bus to inject the desired active and reactive powers to local grid, while the hydropower station will act as a slack bus which maintains its voltage amplitude and frequency. An integrated small-signal state-space model is derived to analyze the system stability of the hybrid microgrid. The simulation results show system frequency and voltage stability for a hybrid microgrid demonstration which includes 2 MWp PV installations, a 15.2 MWh battery system, and a 12.8 MVA hydropower plant. Experimental results on a small-scale laboratory prototype verify the validity of the theoretical analysis and proposed control strategy.

Index Terms-- Hybrid PV-Battery-Hydropower Microgrid, Hierarchical Control, Frequency Stability

I. INTRODUCTION

At present, the electrical utility grid is evolving towards more decentralized architectures and operation, thereby reducing dependency on centralized power plants. A promising decentralized power architecture is the microgrid (MG), which usually involves different kinds of energy sources, such as wind generation or photovoltaic (PV) systems. MGs are local distribution grids, which include different technologies, such as power electronics, distributed generation (DG), control architectures, communication infrastructure, and energy storage systems (ESSs), like flywheels, supercaps or batteries [1], [2].

Islanded hybrid PV-battery-hydropower MGs have been deployed as a practical solution to address local electricity outages, eliminate power fluctuations, and increase the reliability and availability of power supply especially in dry seasons. These hybrid MGs can improve the complementary utilization of different renewable energy sources in remote areas, where the abundant solar irradiance and small scale

hydroelectric power plants are available [3]-[8]. In addition, the seamless transition between grid-connected and islanded modes is usually required for the PV-battery system in hybrid MGs because of the unavailability of the hydropower plant reservoir, such as the run-of-the-river (ROR) projects[9], [10], in which little or no water storage is required.

ESSs are necessary for islanded MGs where the power exchange among the renewable energy sources (RES'), ESS' and loads should be balanced. A number of previous works [11]-[13] indicate that the control capability of ESS is limited by the energy capacity of the energy storage device. If ESS is the only one' responsible for stabilizing the MG, it may result in failure or internal outage. When the different capacities between the hydropower system and the PV-battery system in a hybrid MG are considered, a reasonable solution is for the PV-battery system to operate as a PQ bus to supply the required active and reactive powers to the hydropower-based local grid, while supplying the local loads. The hydropower can operate as a slack bus to establish voltage magnitude and frequency.

In order to achieve the aforementioned, hierarchical control theory is applied to the hybrid MG, thus, providing the functionalities defined in different control levels [14]-[19]. Hierarchical control theory is based on droop control method which has dominated the autonomous control of parallel converters in applications in the last decade such as parallel redundant uninterruptible power supplies, distributed power systems, MGs, and so forth [20], [21]. The droop controller calculates the active and reactive powers of the inverter, and adjusts the local proportional frequency and voltage amplitudes of each inverter to emulate the behavior of a synchronous generator. Some modified droop control strategies have been presented to improve its performance in several applications [22]-[26].

Unlike traditional MGs, the existence of a rotating device makes the islanded PV-battery-hydropower hybrid MG become more complicated. The inertia of hydraulic turbines and generators are decided by the physical dimension and rotor weight. Although this inherent property of rotating device could increase the damping performance of the system, the non-minimum phase system of the hydraulic turbine may result in several instabilities [27]. However, power-

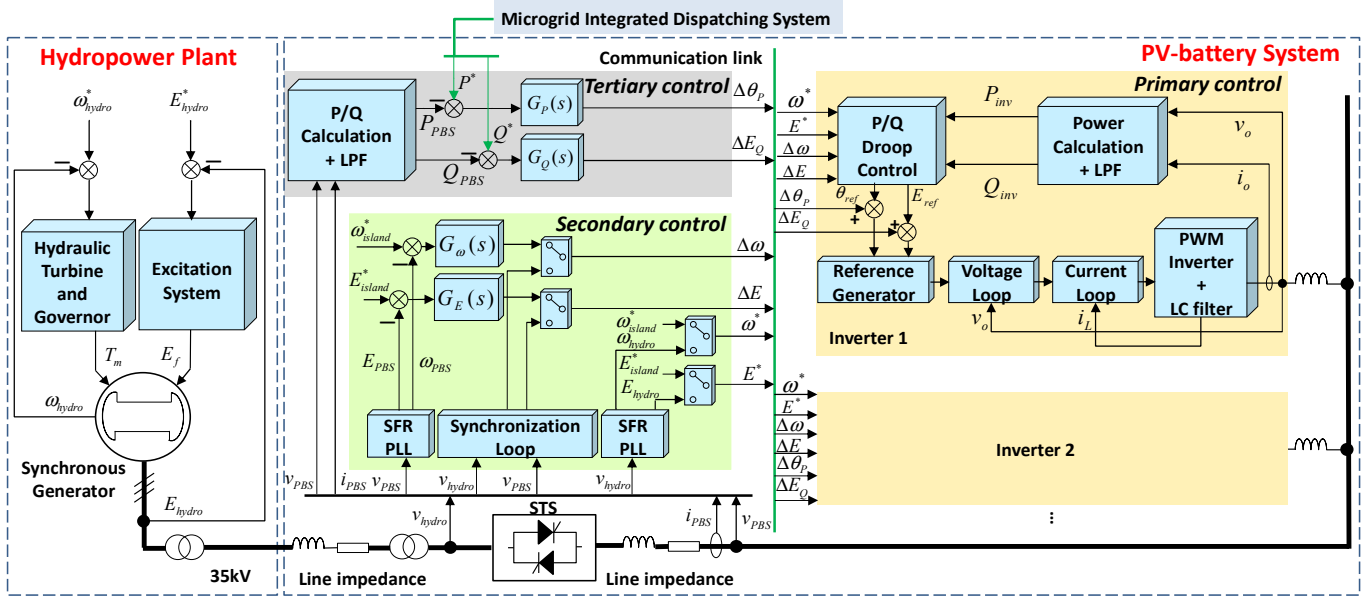


Fig. 1. Block diagram of the islanded hybrid microgrid control

electronics-based MGs are very sensitive to network disturbances because of the absence of physical inertias. In addition, the different transient response speeds of voltage controlled inverter (VCI) and hydropower system may also result in instabilities. Furthermore, the hierarchical control contains a huge number of parameters that needs to be designed, while respecting the trade-offs of stability and transient response performances.

In view of these problems, stability analysis becomes an important issue in hybrid PV-battery-hydropower MGs. The transient stability analysis can be obtained from the relationship between the rotor angles of different energy sources [30]. Additionally, a systematic approach to small-signal modelling of a MG system that includes conventional (rotating machine) and electronically interfaced distributed resource (DR) units is presented [31]. However there are no quantitative conclusions derived from these research works.

Stability analysis based on eigenvalues and root locus plots is presented in previous studies [32]-[37]. A full order small-signal model of a droop controlled MG is derived to analyze system stability in [32]-[35]. However, in these works only inverters are considered. The characteristics of the generators are neglected. By contrast, transient stability of a hydropower plant was studied in [36], [37]. For instance, the small-signal model of a synchronous generator is considered in [36]. Nevertheless, the dynamic response of a hydroelectric power station should be taken into account, since the characteristics of the prime mover and its governor have great influence on the performance of the local electrical network [37].

In this paper, a hierarchical controller for hybrid PV-battery-hydropower MG is proposed. The proposed controller can achieve the parallel operation of PV-battery system and

hydropower station. In order to analyze system stability, an integrated small-signal state-space model is developed. The paper is organized as follows. Section II introduces the configuration of the hybrid power system. Section III develops the integrated linearized system model for both PV-battery system and hydropower station. Section IV analyzes the system stability and parameter sensitivity based on the state-space model. Section V presents frequency and voltage stability analyses based on a real demonstration hybrid MG which includes 2 MWp PV installations, a 15.2 MWh battery system, and a 12.8 MVA hydropower plant. Experimental results on a lab prototype are shown in Section VI to validate the effectiveness of the proposed approach. Section VII concludes the paper.

II. CONFIGURATION OF THE HYBRID POWER SYSTEM

The model of islanded hybrid PV-battery-hydropower MG under study is shown in Fig. 1. The synchronous generator of the hydropower plant provides physical inertia, which differs from conventional power-electronics-based MG.

In this case, the synchronous generator works in standalone mode as a slack bus, which means that the main role of the hydraulic governor and excitation system is to maintain the frequency and voltage amplitude of the hybrid MG. The PV-battery system acts as a PQ bus to inject the desired active and reactive powers to the hydropower-based local grid by means of the proposed hierarchical control which can be divided into three levels [14]-[19].

A. Primary control level

Primary control consists of inner voltage and current control loops, and active power (P) and reactive power (Q) droop control loops. The objectives of primary control are

regulating the frequency and amplitude of the voltage reference provided to the inner voltage and current control loops, adjusting R/X ratio of the output impedance "seen" by the inverter, and sharing the load among VCIs by mimicking the static droop feature of a synchronous generator[20]-[26].

B. Secondary control level

Secondary control includes frequency and voltage restoration control loops and a synchronization loop. Secondary control can compensate the frequency and magnitude deviations to improve the power quality in standalone mode. In addition, the secondary control ensures the synchronization of VCIs' output voltage with the point of common coupling (PCC) voltage before the PV-battery system and hydropower station are connected [38]-[40].

C. Tertiary control level

Tertiary control is responsible for generating the power reference and control VCIs in order to inject dispatched power to hydropower-based local grid, and for optimizing the system [41].

The PV-battery system of the hybrid MG can be seen as a PQ bus. The output voltages of the PV-battery system and the hydropower plant are boosted to 35 kV by using transformers, while the transmission lines between both plants present high X/R ratio. Therefore, P and Q are dominated by power angle (δ) and voltage difference ($V_1 - V_2$), respectively:

$$\delta \approx \frac{XP}{V_1 V_2} \quad (1)$$

$$V_1 - V_2 \approx \frac{XQ}{V_1} \quad (2)$$

where δ is the angle between the hydropower station and the PV-battery system; X is the line impedance; P and Q are the active and reactive power outputs; V_1 and V_2 are the output voltages of hydropower station and PV-battery system.

On the other hand, the frequency of the hydropower system is mainly dominated by the hydraulic governor system and the active power demanded by the load, while the voltage magnitude is mainly dominated by the excitation system and the reactive power demanded by the load. Therefore, the frequency and voltage stability analysis in this paper focuses on studying the relationships between the power flow of PV-battery system and the hydraulic governor as well as the excitation system of the hydropower system.

III. LINEARIZED SYSTEM MODEL

In this Section, a state-space model is presented for the proposed hybrid PV-battery-hydropower system [27]. The hydroelectric power system and the simplified hierarchically controlled PV-battery system include governor, hydraulic turbine, generator, excitation and hierarchical controller,

which are represented by the block diagram shown in Fig. 2. The hydroelectric power system is presented in per-unit.

A. Hydraulic governor

The functionality of the pilot valve and servomotor, and the gate servomotor is to increase the impeller driving signal from a PI controller. The impeller indirectly stabilizes the generator's frequency by controlling the water column. The parallel operation of hydropower can be achieved by using permanent speed droop R_p which endows the $P-\omega$ droop characteristic and determines the slope [42], [43].

The variables of the PI controller, the pilot valve and servomotor, and the gate servomotor can be expressed as:

$$sX_1 = 1 - \omega - R_p X_2 \quad (3)$$

$$sX_2 = \frac{K_{i_hydro}}{T_p} X_1 + \frac{K_{p_hydro}}{T_p} - \frac{K_{p_hydro}}{T_p} \omega - \frac{R_p K_{p_hydro} + 1}{T_p} X_2 \quad (4)$$

$$sX_3 = \frac{1}{T_G} X_2 - \frac{1}{T_G} X_3 \quad (5)$$

where X_1 , X_2 , and X_3 do not have particular physical meanings but they are state variables to facilitate the development of the model; T_p and T_G are the pilot valve and servomotor, and gate servomotor time constant.

The corresponding linearized small-signal state-space equations can be derived from (3)-(5) as follows:

$$\begin{bmatrix} \Delta \hat{X}_1 \\ \Delta X_2 \\ \Delta X_3 \end{bmatrix} = A_{gov} \begin{bmatrix} \Delta X_1 \\ \Delta X_2 \\ \Delta X_3 \end{bmatrix} + B_{gov} [\Delta \omega] \quad (6)$$

being

$$A_{gov} = \begin{bmatrix} 0 & -R_p & 0 \\ K_{i_hydro}/T_p & -R_p K_{p_hydro} + 1/T_p & 0 \\ 0 & 1/T_G & -1/T_G \end{bmatrix}, \quad (7)$$

$$B_{gov} = \begin{bmatrix} -1 \\ -K_{p_hydro}/T_p \\ 0 \end{bmatrix}$$

where Δ denotes the small deviation of the respective variable from the equilibrium point and $\hat{\Delta}$ denotes the derivative with respect to time.

B. Hydraulic turbine

The classical transfer function of an ideal hydraulic turbine can be expressed as:

$$G_{turbine}(s) = \frac{1 - T_w s}{1 + 0.5 T_w s} \quad (8)$$

where T_w is referred to as the water starting time.

The following equations represent the linearized small-signal state-space form of the hydraulic turbine.

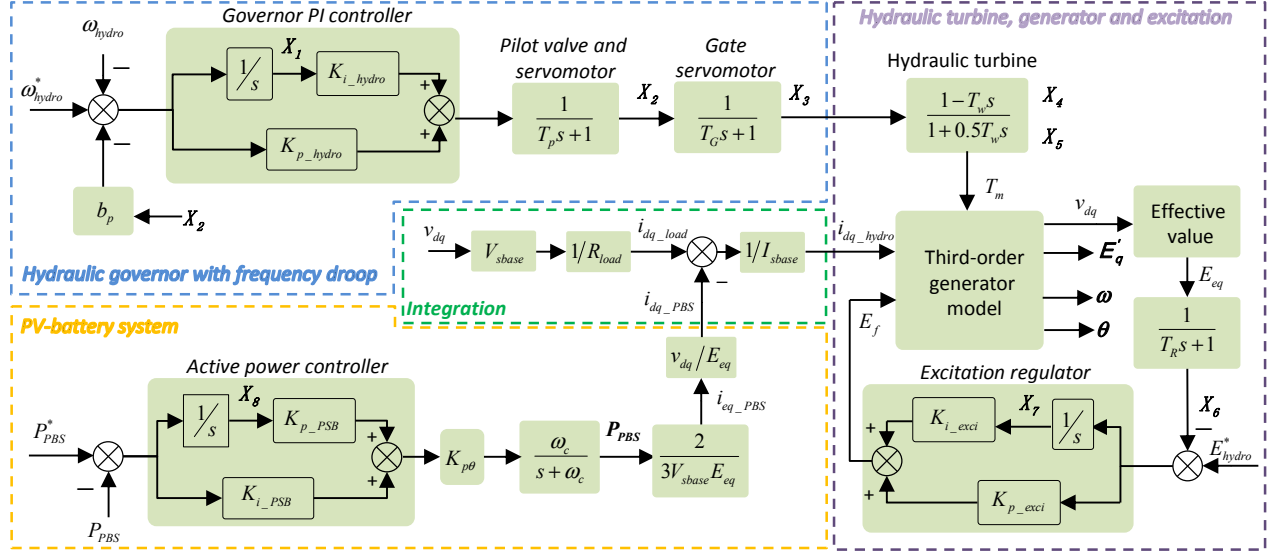


Fig. 2. Block diagram of the small-signal state-space model of the hybrid MG.

$$\begin{bmatrix} \Delta X_4 \\ \Delta X_5 \end{bmatrix} = A_{tur} \begin{bmatrix} \Delta X_4 \\ \Delta X_5 \end{bmatrix} + B_{tur} \Delta X_3 \quad (9)$$

where

$$A_{tur} = \begin{bmatrix} -2/T_w & 0 \\ 0 & -2/T_w \end{bmatrix}, B_{tur} = \begin{bmatrix} 2/T_w \\ 4/T_w \end{bmatrix} \quad (10)$$

The algebraic output equation can be expressed as:

$$[\Delta T_m] = C_{tur1} \begin{bmatrix} \Delta X_4 \\ \Delta X_5 \end{bmatrix} + C_{tur2} \Delta X_3 \quad (11)$$

where T_m is the mechanical input torque.

$$C_{tur1} = [1 \ 1], C_{tur2} = -2 \quad (12)$$

C. Third-order generator model

The classical third-order small-signal state-space form in per unit of synchronous generator [44], [45] is represented as:

$$\begin{bmatrix} \Delta \omega \\ \Delta \theta \\ \Delta E'_q \end{bmatrix} = A_{gen} \begin{bmatrix} \Delta \omega \\ \Delta \theta \\ \Delta E'_q \end{bmatrix} + B_{gen1} \Delta T_m + B_{gen2} \Delta E_f + B_{gen3} \begin{bmatrix} \Delta i_d \\ \Delta i_q \end{bmatrix} \quad (13)$$

$$A_{gen} = \begin{bmatrix} 0 & 0 & -i_q/T_j \\ 0 & 1 & 0 \\ 0 & 0 & -1/T'_{do} \end{bmatrix}, B_{gen1} = \begin{bmatrix} 1/T_j \\ 0 \\ 0 \end{bmatrix}, B_{gen2} = \begin{bmatrix} 0 \\ 0 \\ 1/T'_{do} \end{bmatrix}, \quad (14)$$

$$B_{gen3} = \begin{bmatrix} (X'_d - X_q)i_q/T_j & (X'_d i_d - X_q i_d - E'_q)/T_j \\ 0 & 0 \\ (X'_d - X_d)/T'_{do} & 0 \end{bmatrix}$$

where θ denotes the rotor angle; ω is the angular speed of the generator; $\Delta E'_q$ is the q -axis transient potential; ΔE_f is exciter output voltage; Δi_d and Δi_q are the d -axis and q -axis output currents of generator; T'_{do} is the d -axis time constant; T_j is the inertia constant; X_d and X_q are the synchronous reactance; X'_d and X'_q are the transient reactance.

The generator terminal voltage can be derived as:

$$\begin{bmatrix} \Delta v_d \\ \Delta v_q \end{bmatrix} = C_{gen} \Delta E'_q + D_{gen} \begin{bmatrix} \Delta i_d \\ \Delta i_q \end{bmatrix} \quad (15)$$

being C_{gen} , D_{gen} defined as:

$$C_{gen} = \begin{bmatrix} 0 \\ 1 \end{bmatrix}, D_{gen} = \begin{bmatrix} -r_a & X_q \\ -X'_d & -r_a \end{bmatrix} \quad (16)$$

and r_a as the stator resistance.

D. Excitation system

The basic function of the excitation system is to provide direct current to the synchronous machine field winding. In addition, the excitation system provides control and protective functionalities by means of controlling the field voltage and the field current [27], [46]. In this case, a simplified excitation system is modeled including terminal voltage transducer and excitation regulator.

The root mean square (RMS) value of terminal voltage E_{eq} can be calculated as follow:

$$E_{eq} = \sqrt{v_d^2 + v_q^2} \quad (17)$$

The terminal voltage transducer can be described as:

$$G_{trans}(s) = \frac{1}{T_R s + 1} \quad (18)$$

where T_R represents the terminal voltage transducer time constant.

The excitation regulator can be expressed as follow:

$$G_{exciter_regu}(s) = K_{p_exci} + \frac{K_{i_exci}}{s} \quad (19)$$

where K_{p_exci} and K_{i_exci} represent the proportional and integrated terms of the exciter regulator.

Equations (17) to (19) can be converted to the following small-signal state-space form

$$\begin{bmatrix} \Delta \hat{X}_6 \\ \Delta \hat{X}_7 \end{bmatrix} = A_{exci} \begin{bmatrix} \Delta X_6 \\ \Delta X_7 \end{bmatrix} + B_{exci} \Delta E_{eq} \quad (20)$$

where

$$A_{exci} = \begin{bmatrix} -1/T_R & 0 \\ -1 & 0 \end{bmatrix}, B_{exci} = \begin{bmatrix} 1/T_R \\ 0 \end{bmatrix} \quad (21)$$

The algebraic output equation can be presented as:

$$\Delta E_f = C_{exci} \begin{bmatrix} \Delta X_6 \\ \Delta X_7 \end{bmatrix} \quad (22)$$

$$C_{exci} = \begin{bmatrix} -K_{p_exci} & K_{i_exci} \end{bmatrix} \quad (23)$$

where E_f is the exciter output voltage.

E. Hierarchically-controlled PV-battery system

The P - ω droop controller of the VCI can be expressed as:

$$\omega_{inv} = \omega_{hydro} + \Delta \omega_{syn} - m_p (P_{inv}^* - P_{inv}) \quad (24)$$

$$\theta_{inv} = \int \omega_{inv} dt + \Delta \theta_p \quad (25)$$

where ω_{hydro} is the fundamental value of the P - ω droop controller; $\Delta \omega_{syn}$ is a signal generated by the synchronization controller in secondary control to ensure the synchronization before connecting the VCIs to hydropower-based local grid; m_p is the P - ω droop coefficient; P_{inv}^* is the active power reference; P_{inv} is the active power output of PV-battery system; $\Delta \theta_p$ is generated by a PI regulator in tertiary control in order to ensure that VCIs can inject the dispatched power into the hydropower station-based local grid.

The power transmitted from the PV-battery system to the hydropower plant depends on the power transmission theorem. By considering the predominant inductive line impedances, the active power flow can be expressed by the following equations, with the inductive line impedance:

$$P_{PBS} = K_{p\theta} \sin \Delta \theta_p \quad (26)$$

$$K_{p\theta} = \frac{E_{eq} E_{PBS}}{X_{line}} \quad (27)$$

where P_{PBS} is the active power output of PV-battery system; E_{PBS} is the RMS value of the PV-battery system output voltage, and X_{line} is the equivalent inductive line impedance.

As the bandwidth of the inner voltage and current loops are normally designed at 1/5 to 1/10 of switching frequency, the cutoff frequency of the low pass filter (LPF) in droop control loop are usually 1/10 or even more slower than the

bandwidth of inner loops in order to avoid undesirable interactions. Besides, primary control is usually 6 times faster than the secondary control [39]. Thus, the transient response and control procedure of the droop controller and the inner loops should be faster enough to be neglected compared with the tertiary control and the governor dynamics.

The major issue that may affect the system stability and the transient response is the communication fault of the tertiary and secondary control. Some previous works [39], [40] investigated the impact of communication latency of the secondary control in MGs. In [39], both centralized and decentralized controllers present good performance for a time delay of 200ms (about 10 line cycles). In view of this case, the centralized secondary control is employed, thus, it has the capability to maintain the proper operation with latencies of less than 1 s [39]. Therefore, the hierarchically-controlled PV-battery system in this case can be simplified as shown in Fig. 2, which includes the PI regulator in tertiary control, the power transmitted loop $K_{p\theta}$, and a LPF which represented the simplified droop control loop and inner voltage and current loops.

Therefore, the corresponding linearized small-signal state-space equations can be derived from (26), (27) as:

$$\begin{bmatrix} \Delta \hat{X}_8 \\ \Delta P_{PBS} \end{bmatrix} = A_{PBS} \begin{bmatrix} \Delta X_8 \\ \Delta P_{PBS} \end{bmatrix} \quad (28)$$

$$A_{PBS} = \begin{bmatrix} 0 & -1 \\ K_{i_PBS} K_{p\theta} \omega_c & -(K_{p_PBS} K_{p\theta} \omega_c + \omega_c) \end{bmatrix} \quad (30)$$

where K_{p_PBS} and K_{i_PBS} are the parameters of the PI controller in tertiary control; ω_c is the bandwidth of LPF.

F. Combined model of hybrid MG

A mathematical transformation is necessary to combine the hydropower station and PV-battery system models. The transformation is based on the relationship between PV-battery system output current and the hydropower station output current based on Kirchhoff's current law, as the load current should equal to the sum of PV-battery system output current and hydropower station output current as shown in integration part of Fig. 2.

$$(\Delta i_{dq_load} - \Delta i_{dq_PBS}) \frac{1}{I_{sbase}} = \Delta i_{dq_hydro} \quad (31)$$

where I_{sbase} is the base value of generator output current.

Hypothetically, the amplitude of generator's output voltage E_{eq} can be assigned to 1, by means of excitation regulator. The small-signal form of PV-battery system output current in dq reference frame can be expressed as follow:

$$\Delta i_{dq_PBS} = \frac{2 \Delta P_{PBS} v_{dq} + P_{PBS} \Delta v_{dq}}{3 V_{sbase}} \quad (32)$$

where V_{sbase} is the base value of generator output voltage.

The output current of hydropower is equal to the

difference of load current and PV-battery system output current. Thus, the small-signal state-space form of the hydropower output current can be presented as:

$$\begin{bmatrix} \Delta i_d \\ \Delta i_q \end{bmatrix} = C_{i1} \Delta P_{PBS} + C_{i2} \Delta E'_q \quad (33)$$

$$C_{i1} = \begin{bmatrix} K_a \\ K_c \end{bmatrix}, C_{i2} = \begin{bmatrix} K_b \\ K_d \end{bmatrix} \quad (34)$$

where K_a, K_b, K_c and K_d are constants.

The small-signal dynamics of the terminal voltage can be derived from (17) as follows:

$$\Delta E_{eq} = K_{eq} \begin{bmatrix} \Delta v_d \\ \Delta v_q \end{bmatrix} \quad (35)$$

$$K_{eq} = \begin{bmatrix} v_d (v_d^2 + v_q^2)^{-1/2} & v_q (v_d^2 + v_q^2)^{-1/2} \end{bmatrix} \quad (36)$$

By substituting $\Delta v_d, \Delta v_q, \Delta i_d,$ and Δi_q from (15) to (33), the small-signal form in (35) can be rearranged as:

$$\Delta E_{eq} = (K_{eq} C_{gen} + K_{eq} D_{gen} C_{i2}) \Delta E'_q + K_{eq} D_{gen} C_{i1} \Delta P_{PBS} \quad (37)$$

Based on (3)-(37), a complete state-space small-signal model of the hybrid PV-battery-hydropower MG can be obtained by combining the sub-state-space models of the hydraulic governor, hydraulic turbine, generator, excitation, hierarchically controlled PV-battery system, and transformation and integration model, which are given by (6), (9), (13), (20) and (28). The hybrid power system has a total of 12states.

$$[\Delta \hat{X}] = A[\Delta X] \quad (38)$$

being

$$[\Delta X] = [\Delta X_1 \quad \Delta X_2 \quad \Delta X_3 \quad \Delta X_4 \quad \Delta X_5 \quad \Delta \omega \quad \Delta \theta \quad \Delta E'_q \quad \Delta X_6 \quad \Delta X_7 \quad \Delta X_8 \quad \Delta P_{PBS}]$$

$$A = \begin{bmatrix} A_{11} & 0 & A_{13} & 0 & 0 \\ A_{21} & A_{22} & 0 & 0 & 0 \\ A_{31} & A_{32} & A_{33} & A_{34} & A_{35} \\ 0 & 0 & A_{43} & A_{44} & A_{45} \\ 0 & 0 & 0 & 0 & A_{55} \end{bmatrix}, A_{11} = A_{gov},$$

$$A_{13} = [B_{gov} \quad 0 \quad 0], A_{21} = [0 \quad 0 \quad B_{tur}], A_{22} = A_{tur},$$

$$A_{31} = B_{gen1} [0 \quad 0 \quad C_{tur2}], A_{32} = B_{gen1} C_{tur1},$$

$$A_{33} = A_{gen} + B_{gen3} [0 \quad 0 \quad C_{i2}], A_{34} = B_{gen2} C_{exci},$$

$$A_{35} = B_{gen3} [0 \quad C_{i1}],$$

$$A_{43} = B_{exci} [0 \quad 0 \quad K_{eq} C_{gen} + K_{eq} D_{gen} C_{i2}], A_{44} = A_{exci},$$

$$A_{45} = B_{exci} [0 \quad K_{eq} D_{gen} C_{i1}], A_{55} = A_{PBS}.$$

IV. STABILITY ANALYSIS BASED ON LINEARIZED MODEL

In order to analyze and to ensure system stability, as well as to adjust the transient response of the hybrid system, the eigenvalues of (38) are represented along several root locus

plots as a function of different parameter variations. The system parameters and equilibrium point are listed in Table I.

Fig. 3 shows the root locus plot for the system by considering a variation of the proportional term of the hydraulic governor regulator K_{p_hydro} from 10^{-3} to 10^{-1} . It can be seen that the system response becomes underdamped when increasing K_{p_hydro} . In this case, the system will become unstable when K_{p_hydro} increases beyond 2.5.

Fig. 4 shows the root locus plot for the system as a function of the variation of the proportional term in excitation system regulator K_{p_exci} from 0.01 to 3. The system has an underdamped response for higher values of K_{p_exci} . The system can maintain stability as the eigenvalues are displaced only within the left hand plane. Therefore, K_{p_exci} can be varied in a wider range in comparison with K_{p_hydro} .

Fig. 5 shows the root locus plot for the system corresponding to a variation of terminal voltage transducer time constant T_R in the range of 10^{-3} to 10^{-1} . The figure shows that increasing T_R leads to one pair of complex conjugated poles λ_8 and λ_9 , which are split as two real poles. The single pole is attracted toward the origin, while maintaining the poles in the left half plane.

Fig. 6 shows the root locus plot for the system considering a variation of proportional term of tertiary controller in PV system K_{p_PBS} from 10^{-5} to 10^{-3} . As K_{p_PBS} increases, the single pole becomes attracted to the origin without any oscillation. Thus, system behavior can be regarded as a first-order system but it turns slower. As the pole remains in the left half plane, the system is stable in the range of concern.

Fig. 7 shows the root locus plot for the system considering a variation of cutoff frequency of LPF in PV system ω_c from 0.01 to 100. As ω_c increases, the single pole tends to

TABLE I
MODEL PARAMETERS AND EQUILIBRIUM POINT

Model Parameters					
Symbol	values	Symbol	values	Symbol	values
K_{p_hydro}	1	T_J	5.6812	T_R	1e-3
K_{t_hydro}	0.05	T'_{do}	0.012	K_{p_exci}	0.05
R_p	0.005	X_d	1.8	K_{t_exci}	0.5
T_p	0.005s	X_q	0.895	K_{p_PBS}	0.02
T_G	0.05s	X'_d	0.184	K_{t_PBS}	0.10
T_w	2.0s	r_a	0.082	K_{pq}	1.08e+5
K_a	1.1e-05	K_c	-1.24e-04	ω_c	50 rad/s
K_b	0.0022	ω_{abase}	100pi rad/s	K_d	-0.0496
V_{abase}	326.5986	R_{load}	100 Ω		
Equilibrium Point					
Symbol	values	Symbol	values	Symbol	values
ω^*	1rad/s	i_d	0.0022	i_q	-0.0493
E'_q	0.9954	u_d	-0.0443	u_q	0.999

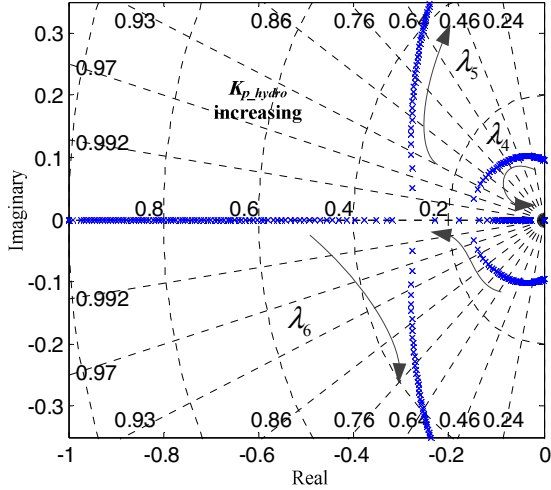


Fig. 3 Trace of modes as a function of proportional term of hydraulic governor regulator: $10^{-3} < K_{p_hydro} < 0.1$.

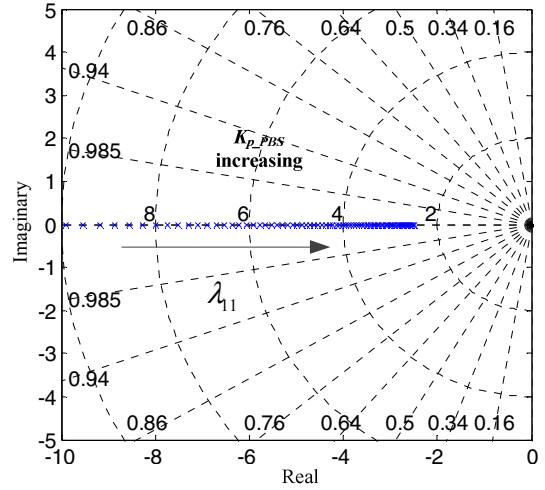


Fig. 6 Trace of modes as a function of proportional term of tertiary controller in PV-battery system: $10^{-5} < K_{p_PBS} < 10^{-3}$.

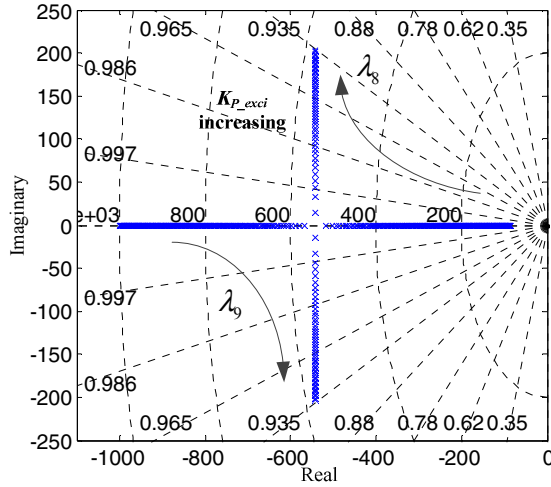


Fig. 4 Trace of modes as a function of proportional term of excitation system regulator: $0.01 < K_{p_excit} < 3$.

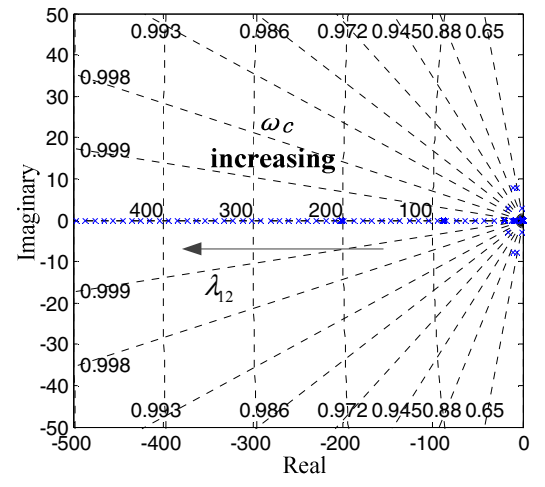


Fig. 7 Trace of modes as a function of cutoff frequency of LPF in PV system: $0.01 < \omega_c < 100$.

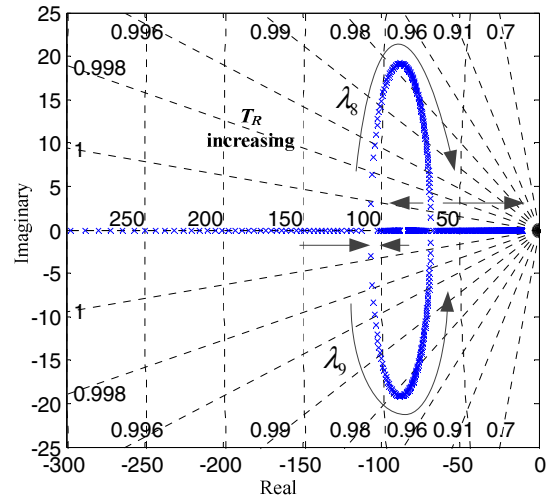


Fig. 5 Trace of modes as a function of terminal voltage transducer time constant: $10^{-3} < T_R < 0.1$.

move far away from the origin without any oscillation. Note that, the higher the cutoff frequency, the faster the system response is. Therefore, the tradeoff between the response speed and the interaction between the inner voltage and current controllers has to be taken into account when the cutoff frequency of the LPF is designed.

V. FREQUENCY AND VOLTAGE STABILITY ANALYSIS BASED ON A DEMONSTRATION OF HYBRID MICROGRID

In this Section, system frequency and voltage stabilities are analyzed using simulation models based on a demonstration hybrid MG, which include 2 MWp of PV, a 15.2 MWh lead-acid battery system, and a 12.8 MVA hydropower plant under several case-study scenarios. The hybrid MG used in this paper is shown in Fig. 8.

Figs. 9(a) and (b) show the transient response of system frequency and voltage when 1 MW load is connected to the hybrid MG at $t=100$ s. After 60 s of oscillation, the system

frequency finally stabilized at 49.79 Hz, while the 35 kV bus voltage of the hybrid MG stabilized at 34.46 kV. The voltage and frequency drops resulting from the step change of the output active power can be compensated by increasing the hydropower plant's voltage and frequency per unit references.

Figs. 10(a) and (b) show the transient response of system frequency and voltage when 1 MW load is disconnected from the hybrid MG at $t=200$ s. After 50 s oscillations, the system frequency is finally restored to 49.98 Hz, while, the 35 kV bus voltage is restored to 34.79 kV.

Fig. 11(a) shows the transient response of system frequency when solar irradiance suddenly dropped to 30% at $t=100$ s. After about 70 s oscillations, system frequency finally stabilized at 49.98 Hz, which is almost same as the system frequency before the solar irradiance drop. Fig. 10(b) illustrates the 35 kV bus voltage variations. After about 70 s oscillations, the voltage stabilized at 34.81 kV. Fig. 10(c) presents the output power transient response of one of the PV-battery stations in parallel when solar irradiance suddenly dropped to 30% at $t=100$ s. Notice that the active power output of the VCIs is reduced by 19.74% (197.4 kW) at 100 s. After about 60 s oscillations, the active power output is restored to the nominal value (1MW) by means of discharging the battery storage system.

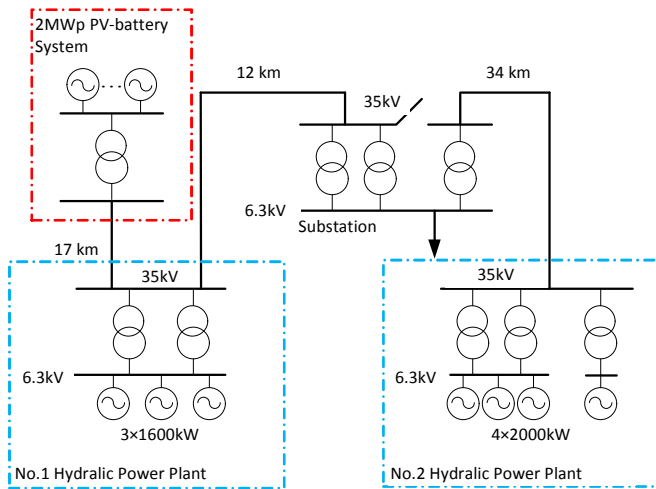


Fig. 8. Electrical diagram of the demonstration hybrid microgrid.

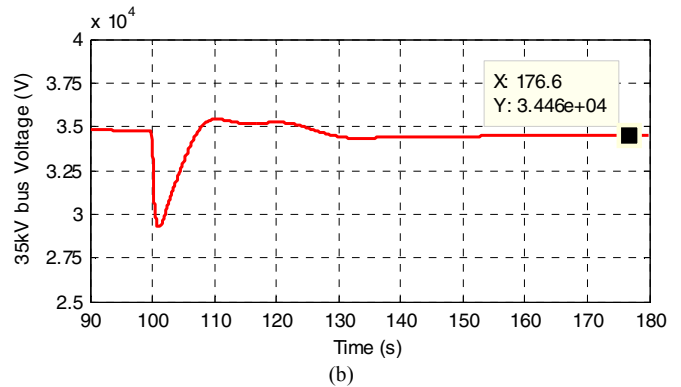
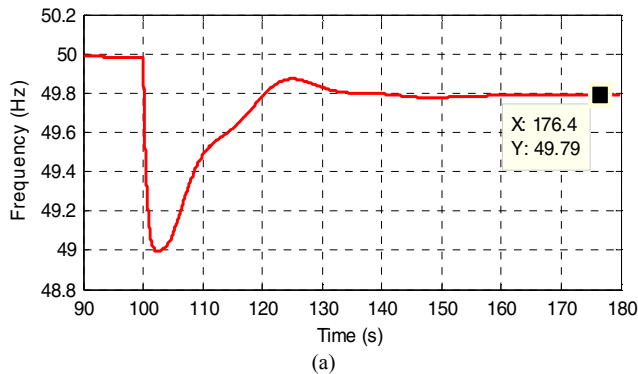


Fig.9. Transient response during step up load disturbance. (a) Frequency, (b) 35kV bus voltage.

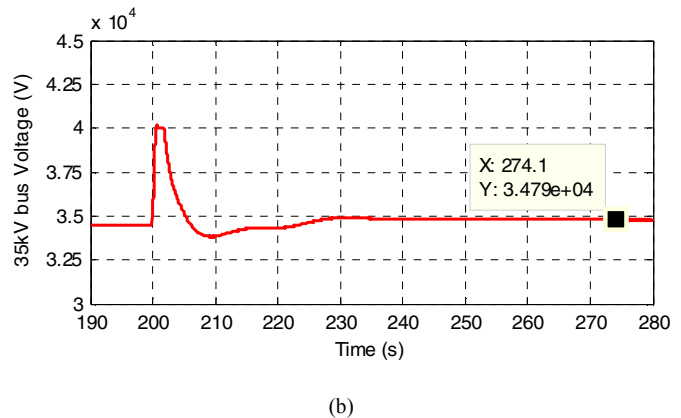
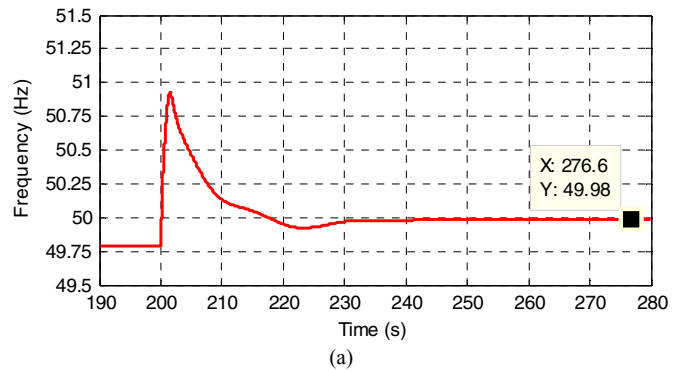
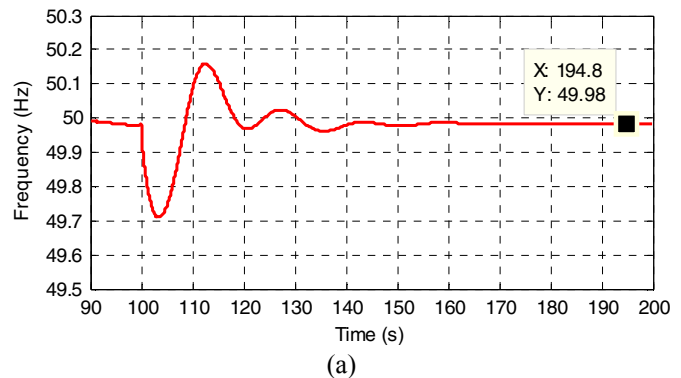


Fig.10. Transient response during step down load disturbance. (a) Frequency, (b) 35kV bus voltage.



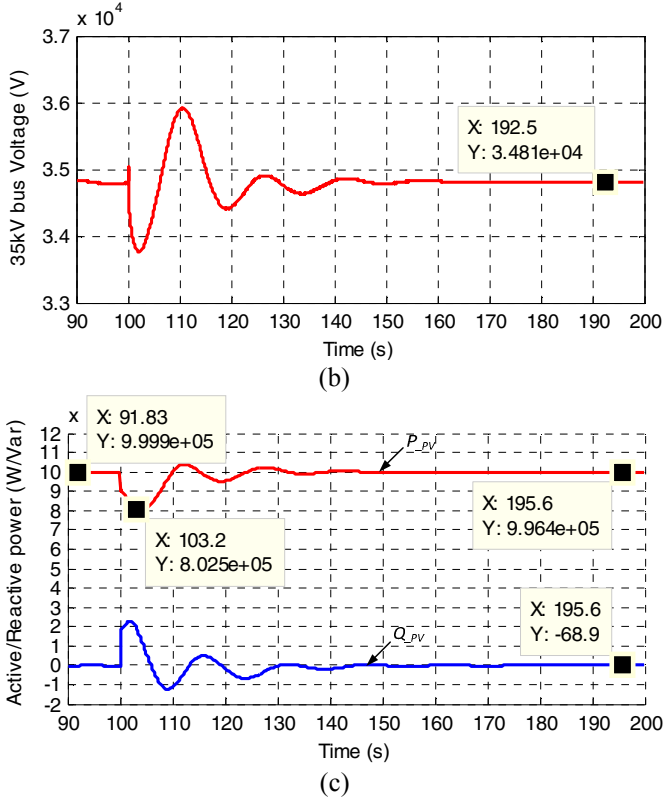


Fig. 11. Transient response during solar irradiance drop. (a) Frequency, (b) 35kV bus voltage, (c) Output power of PV-battery system.

VI. EXPERIMENTAL RESULTS

An experimental hybrid MG setup consists of two three-phase inverters formed as a hybrid PV-battery-hydropower MG, as shown in Fig. 12. This was used to verify the validity of theoretical analysis about the frequency stability and to test the performance of the proposed hierarchical controller. Fig.

13 shows the overall control scheme of the experimental platform. This includes two Danfoss 2.2 kW inverters, a dSPACE1006 real-time control and acquisition platform, LCL filters, and LEM sensors. Three 2 kW resistors are connected to each inverter to simulate different loading conditions. An LR line impedance is connected between two inverters. The switching frequency is 10 kHz.

In this setup, inverter 1 is used to simulate the hydropower station. The proposed hierarchical control is implemented in the other unit to simulate the VCI interfaced PV-battery system. The electrical setup and control system parameters are listed in Table I and Table II. Different case-study scenarios have been considered to validate the proposed controller.

A. Hot-swap operation

Fig.14 shows the transient response when the PV-battery

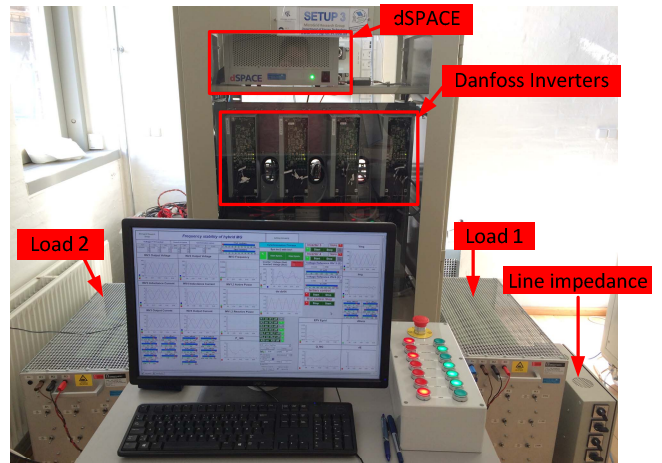


Fig. 12. Experimental setup

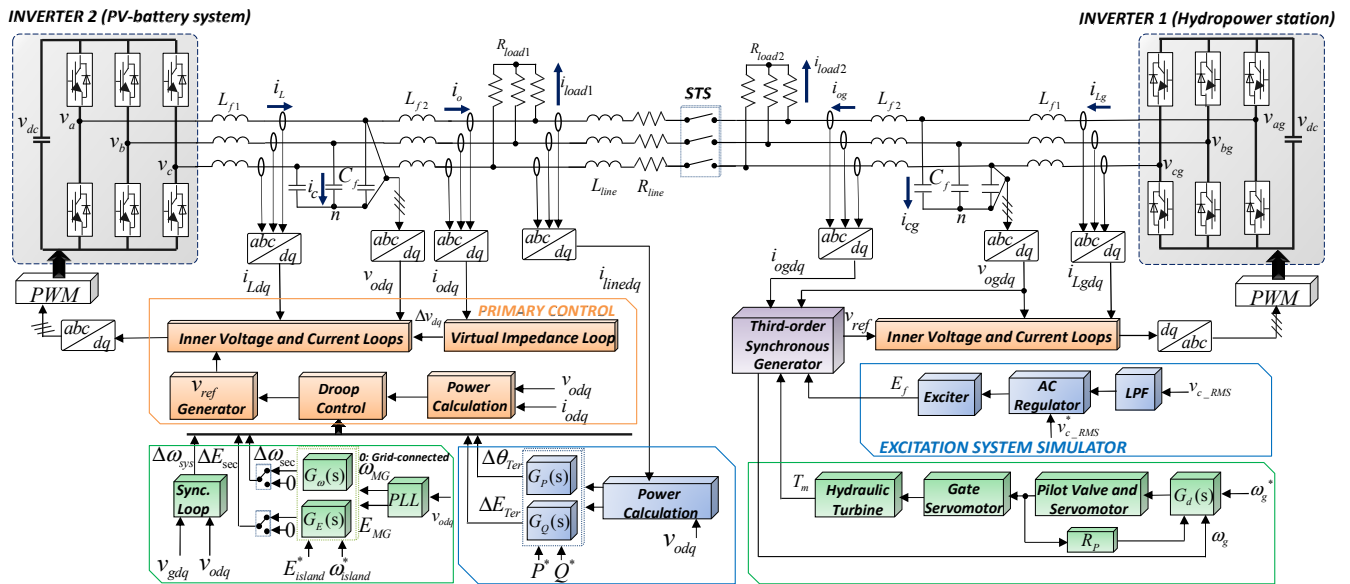


Fig. 13 Overview control scheme.

TABLE II
POWER STAGE AND CONTROL SYSTEM PARAMETERS

Parameters		Value
Symbol	Description	
DG Inverter, Output Filter and Line Impedance		
V_{dc}	DC Voltage	650 V
V_{MG}	MG Voltage	311 V
f	MG Frequency	50 Hz
f_s	Switching Frequency	10k Hz
L_{f1}	Filter Inductance	1.8 mH
C_f	Filter Capacitance	25 μ F
L_{f2}	Filter Inductance	1.8 mH
L_{line}	Line impedance	1.5 mH
r_{line}	Line impedance	0.4 Ω
Loads		
R_{load1}	Local Load 1	115 Ω / 230 Ω
R_{load2}	Local Load 2	230 Ω / 460 Ω
R_{load2}	Step up/ down load	460 Ω
Inner Loops		
k_{pi}	Current proportional term	0.07
K_{ii}	Current integral term	0
K_{pv}	Voltage proportional term	0.04
K_{iv}	Voltage integral term	94
Power Droop Control		
k_{pP}	Active power droop proportional coefficient	5e-7
k_{iP}	Active power droop integral coefficient	6e-6
k_{pQ}	Reactive power droop proportional coefficient	1e-5
k_{iQ}	Reactive power droop integral coefficient	0
Secondary Control		
k_{p_s}	Frequency proportional term	0.00059
k_{i_s}	Frequency integral term	0.0001
$k_{p_{s_A}}$	Amplitude proportional term	0.001
$k_{i_{s_A}}$	Amplitude integral term	0.1
Tertiary Control		
K_{pp_Ter}	Active power proportional term	3e-4
K_{pi_Ter}	Active power integral term	25e-4
K_{qp_Ter}	Reactive power proportional term	1e-3
K_{qi_Ter}	Reactive power integral term	1e-2

system is connected to the hydropower plant. As it can be observed in this figure, DG units are operating with different power rates. The hydropower unit is connected to a 115 Ω load feeding around 1200 W. On the other hand, the PV-battery system is connected to a 230 Ω load feeding around 626 W. After the synchronization process, DG units are connected at 7.7 s, operating in parallel like an islanded MG.

It is worth noting that the output powers of both units nearly maintain their previous values after the connection. The reason of this is that the power reference value in the tertiary control is preassigned to zero in order to reduce overshoots during the connection process. At 13.5 s, the tertiary control starts to act by increasing the power reference value to 130 W. It can be seen that the output power of the PV-battery system is increased by 130 W, while the output power of hydropower station is decreased also by 130 W, as shown in Fig. 14(b). The tertiary controller successfully controls the output power of PV to the desired value. The maximum active power overshoot in Fig. 14(b) is 0.17 per-unit. Fig. 14(a) shows the frequency response of both DG units during the connecting process. After about 85 s, the system frequency is restored to 49.987 Hz due to the compensation of the output power from PV-battery system. The frequency overshoot is very small. As can be observed, even with different power rates and power sources, the DG units with the proposed control strategy will still maintain stable parallel operation to regulate successfully the output power and system frequency. Fig. 14(c) shows the reactive power sharing performance. As seen that 150 Var reactive power is exchanged between DGs even though the power step-up change is in active power, because the presence of the resistive part in the RL line impedances and the lines. This effect can be reduced by increasing the voltage magnitude droop coefficient in the primary control at the expense of reducing the voltage quality. The details of the transient process can be found in each sub-figure.

Fig.15 shows the transient response when the PV-battery system is disconnected from the hydropower plant. As it can be seen, the PV-battery system is disconnected from the hydropower station at 16.88 s, and the tertiary control is disabled. Fig. 15 (a) illustrates the frequency response of two DG units. The frequency of PV-battery system is restored to nearly 50Hz in about 4 s. The deviation of PV-battery system frequency is determined by the $P-\omega$ droop coefficient and the output power. Meanwhile, the frequency of hydropower station decreases from 49.987 Hz to 49.985 Hz after around 50 s because of the PV output power withdraw and hydraulic output power increase. As can be observed, the output power of hydropower system is increased immediately to supply the total amount of local load. At the same time, the output power of PV-battery system is decreased to its original value as the tertiary control is turned off. Fig. 15(c) illustrates the obtained reactive power sharing performance.

B. Load disturbances in hydropower side

Fig. 16 shows the transient response for a load step-up change in the hydropower station side. At the beginning, the DG units are operating in parallel with different power rates. The hydropower station is connected to a 230 Ω load. However it is feeding around 490 W because the PV-battery system supplies 120 W by means of the tertiary control. The PV-battery system is connected to 460 Ω load feeding of

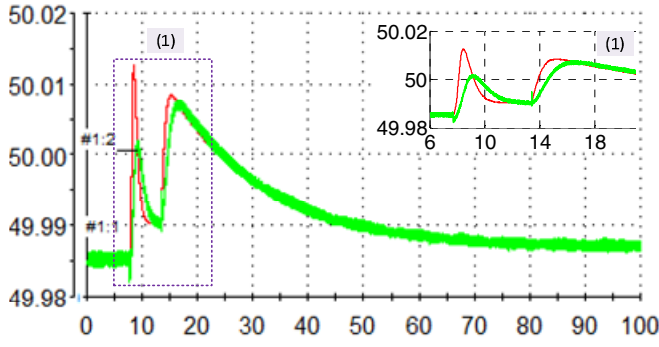


Fig. 14. Transient response when PV-battery system is connected to hydro power station: (a) frequency; (b) active power response; (c) reactive power response. Hydro power station (red) and PV-battery system (green).

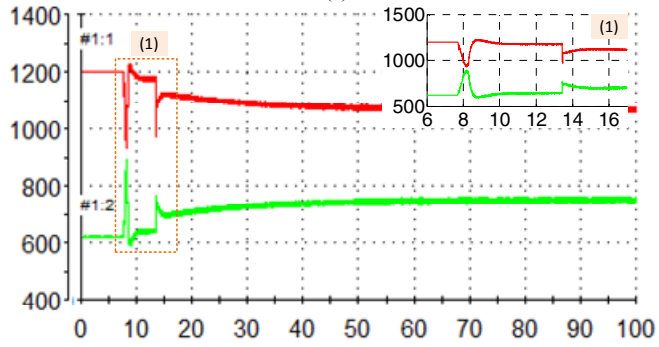


Fig. 14. Transient response when PV-battery system is connected to hydro power station: (a) frequency; (b) active power response; (c) reactive power response. Hydro power station (red) and PV-battery system (green).

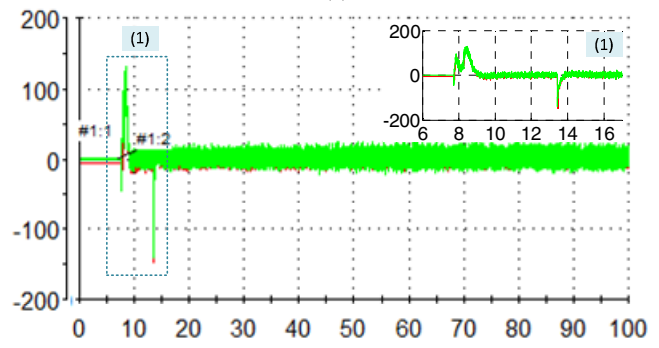


Fig. 14. Transient response when PV-battery system is connected to hydro power station: (a) frequency; (b) active power response; (c) reactive power response. Hydro power station (red) and PV-battery system (green).

around 430 W, which includes the extra 120 W caused by tertiary control. At 8.6 s, another extra 460 Ω load is connected to the hydro power station side, which causes around 310 W of real power step change. Note that the real power output of hydro power station increases by 310 W in 90 s to supply the needed current as shown in Fig.16 (b). Whereas, the active power output of the PV-battery system is finally restored to its original value with nearly no increase thanks to the hierarchical controller. The output power of PV-battery is barely affected by the hydro power station-side load step-up disturbance. The maximum active power overshoot

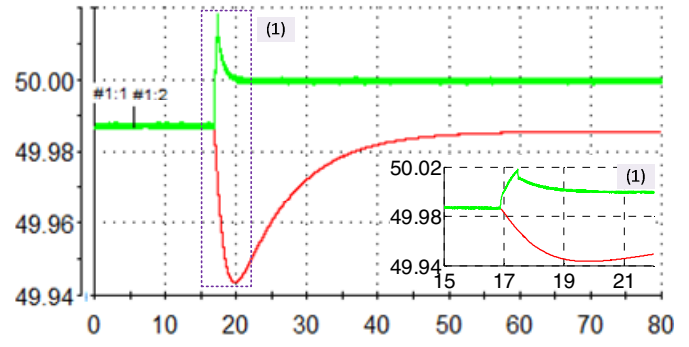


Fig. 15. Transient response when PV-battery system is disconnected from hydro power station: (a) frequency; (b) active power response; (c) reactive power response. Hydro power station (red) and PV-battery system (green).

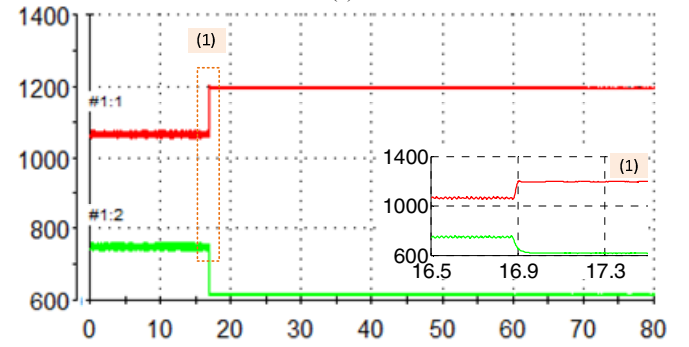


Fig. 15. Transient response when PV-battery system is disconnected from hydro power station: (a) frequency; (b) active power response; (c) reactive power response. Hydro power station (red) and PV-battery system (green).

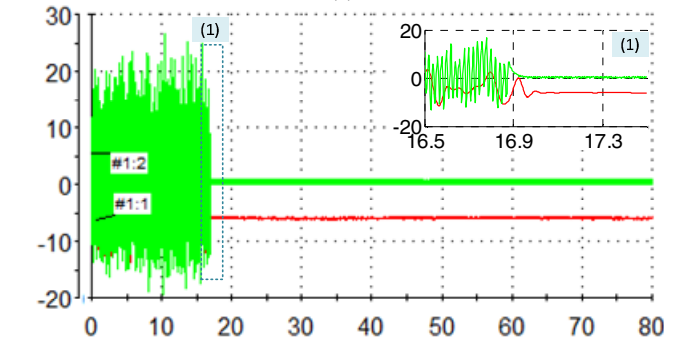
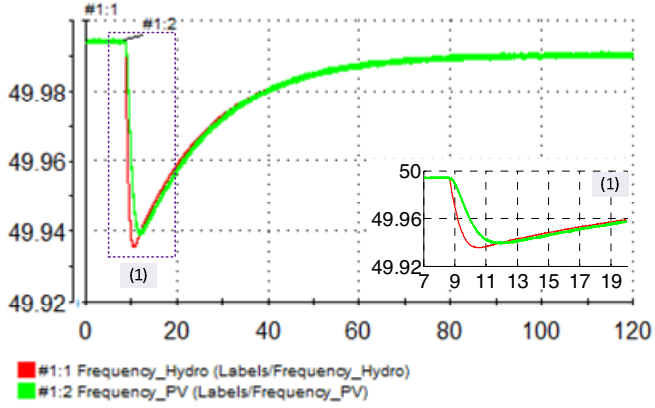


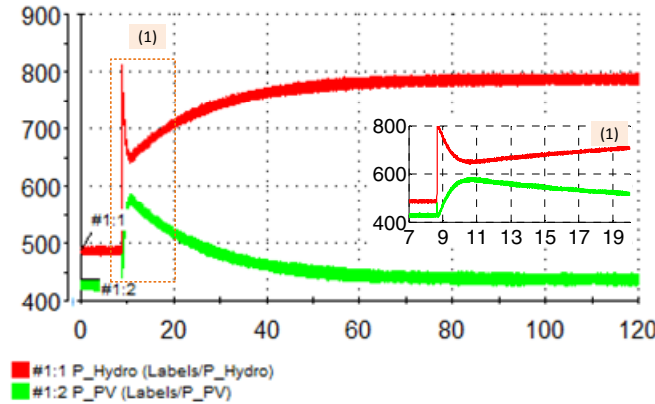
Fig. 15. Transient response when PV-battery system is disconnected from hydro power station: (a) frequency; (b) active power response; (c) reactive power response. Hydro power station (red) and PV-battery system (green).

in Fig. 16(b) is 0.37 per-unit that caused by the oscillation of system frequency. Fig. 16(a) depicts the frequency response to the load disturbance for both DG units. It can be seen the system frequency decreased from 49.995 to 49.99 Hz due to the increase of the hydraulic output power. The frequency overshoot is 0.00088 per-unit. Note that, the system frequency is determined by hydro power station, which is operated as voltage reference bus. Fig. 16(c) illustrates the reactive power response. There is also a large overshoot which can be reduced at the expense of voltage quality.

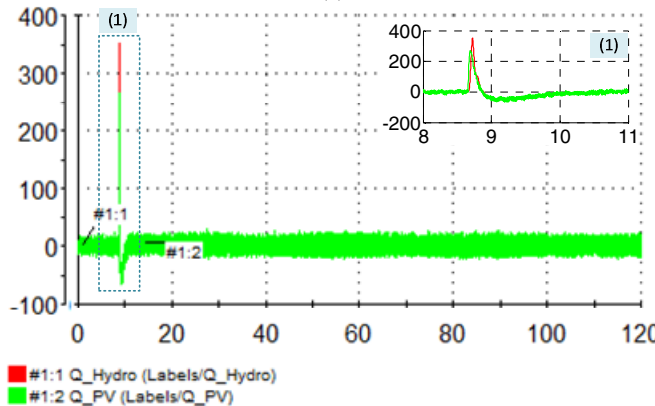
Figs.17 shows the transient process to a load step-down change in hydro power station side. As can be observed in this



(a)



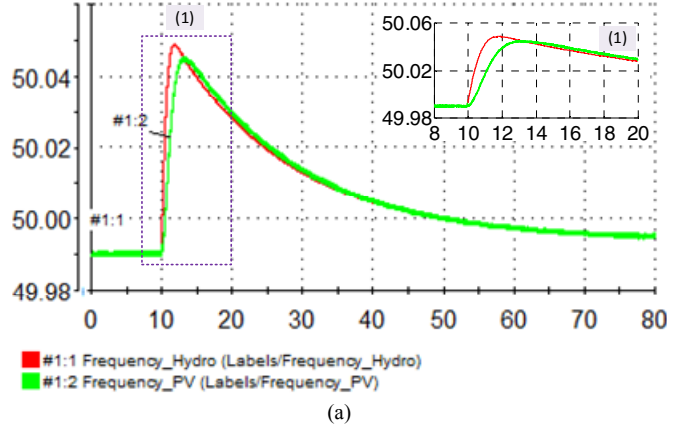
(b)



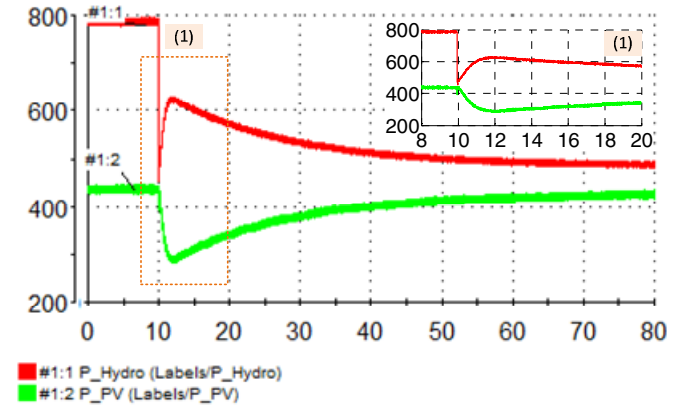
(c)

Fig. 16. Transient responses to a load step up change in hydropower station side: (a) frequency; (b) active power response; (c) reactive power response. Hydropower station (red) and PV-battery system (green).

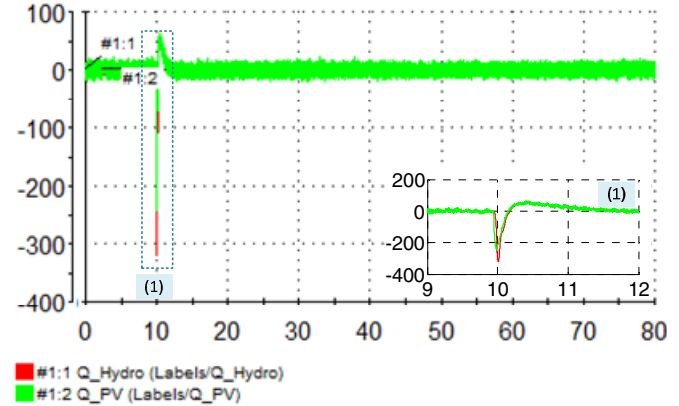
figure, the original operation state is the end of the last test as shown in Fig. 16. At 10 s, the 460 Ω load was disconnected from the hydropower station side, which results in around 310 W of real power step down. The real power output of hydropower station decreases to 485 W, as shown in Fig.17 (b). By contrast, the active power output of PV-battery system is finally restored to its original value without nearly any change due to the hierarchical controller. Fig. 17(a) depicts the frequency response to the load disturbance for both DG units. System frequency has increased from 49.99 to 49.995 Hz due to the decrease in hydraulic output power. The



(a)



(b)



(c)

Fig. 17. Transient responses to a load step down change in hydropower station side: (a) frequency; (b) active power response; (c) reactive power response. Hydropower station (red) and PV-battery system (green).

frequency overshoot is 0.001 per-unit. Fig. 17(c) illustrates the reactive power response.

C. Load disturbances in PV-battery system side

Fig.18 shows the transient response for load step-up and step-down changes in PV-battery system side. At the beginning, the DG units have the same parallel operation states with scenario B, in where the hydropower station feeds are around 490 W and the PV-battery system feeds are around 430 W. At 10.26 s, another 460 Ω load is connected to the PV-battery system side, which causes around 310 W of

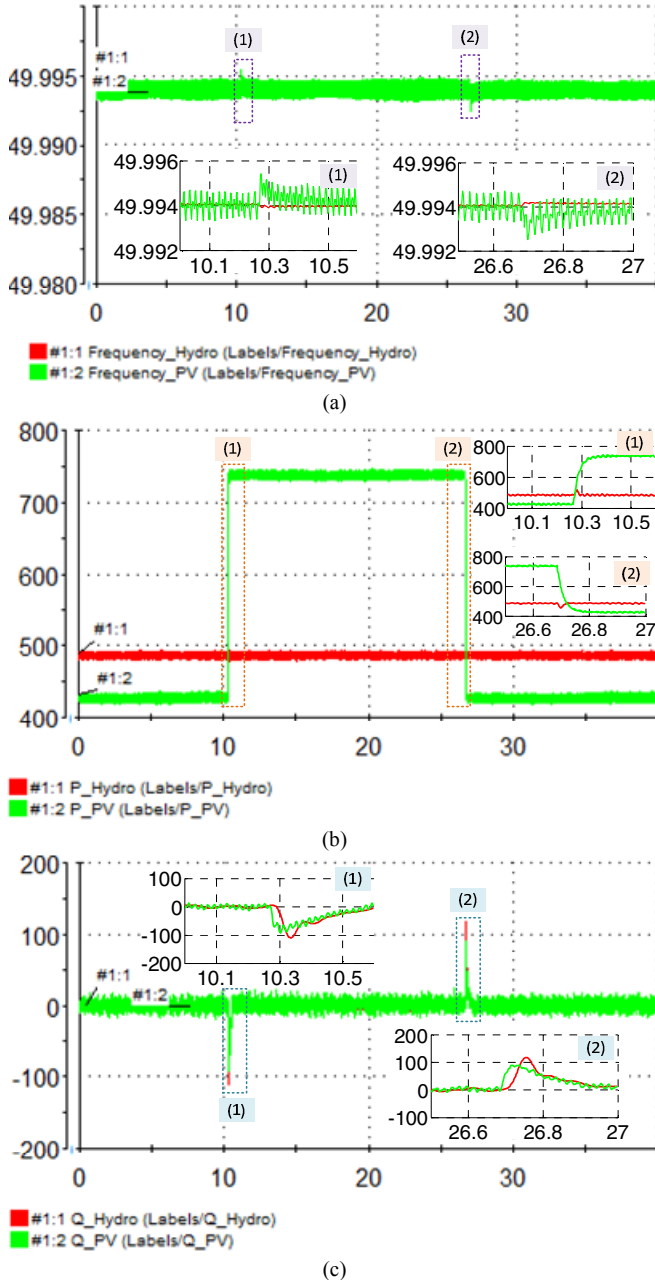


Fig. 18. Transient responses to a load step up/down changes in PV-battery system side: (a) frequency; (b) active power response; (c) reactive power response. Hydropower station (red) and PV-battery system (green).

real power step-up change. As can be observed in Fig 18(b), the real power output of PV-battery system increases immediately by 310 W to supply the needed current. Meanwhile, the active power output of hydropower station is kept constant since the injected power from PV-battery system to hydropower station is controlled at a constant value (120W) by means of the tertiary controller. Fig. 18(a) shows the frequency response to the load step changes. As the system frequency is determined by the hydropower, the responses of both DGs' frequencies are nearly constant, except for two small overshoots in PV-battery system

frequency when the load steps up and down. At 26.69 s, the 460 Ω load is disconnected from the side of PV-battery system. It can be seen that the active power output of PV-battery system is immediately decreased to the original value 430W without change on hydraulic active power output. Fig. 18(c) shows the reactive power response of both DG units.

These tests show that the proposed control strategy can achieve not only a proper parallel operation of the hydropower station and the PV-battery system with different power rates and control methods, but can also completely decouple the control of the active power output of different DG units.

VII. CONCLUSION

This paper proposed a hierarchical controller for islanded hybrid PV-battery-hydropower MG to achieve parallel operation of hydropower station and PV-battery system with different power rates. The proposed controller achieves a complete decoupling power control between hydropower station and PV-battery system. An integrated small-signal state-space models for both hydroelectric power and PV-battery system were developed to analyze the stability of the hybrid MG. Root locus plots are also presented to help identify the origin of each mode to improve system stability. Frequency and voltage simulation results were obtained from an islanded hybrid MG demonstration by considering several case-study scenarios. Experimental results validate the effectiveness of the proposed approach.

REFERENCES

- [1] Guerrero, J.M.; Poh Chiang Loh; Tzung-Lin Lee; Chandorkar, M., "Advanced Control Architectures for Intelligent Microgrids—Part II: Power Quality, Energy Storage, and AC/DC Microgrids," *Industrial Electronics, IEEE Transactions on*, vol.60, no.4, pp.1263,1270, April 2013.
- [2] Lasseter, R.H., "MicroGrids," *Power Engineering Society Winter Meeting, 2002. IEEE*, vol.1, no., pp.305-308, 2002.
- [3] Wu Chun Sheng; Liao Hua; Yang Zi Long; Wang Yi Bo; Peng Yan Chang; Xu Hong Hua, "Research on control strategies of small-hydro/PV hybrid power system," *Sustainable Power Generation and Supply*, pp.1-5. 2009.
- [4] Kusakana, K., Munda, J.L., Jimoh, A.A., "Feasibility study of a hybrid PV-micro hydro system for rural electrification," *AFRICON '09*, pp. 1-5, Sept. 2009.
- [5] Zhou, J.H., Ge, X.H.; Zhang, X.S., Gao, X.Q. and Liu, Y., "Stability simulation of a MW-scale PV-small hydro autonomous hybrid system," *Power and Energy Society General Meeting (PES)*, pp. 1-5. 2013.
- [6] Wang Yibo, Xu Honghua, "Research and Practice of Designing Hydro/Photovoltaic Hybrid Power System in Microgrid," *Photovoltaic Specialists Conference (PVSC)*, pp. 1509-1514. 2013
- [7] Priolkar, J.G., Doolla, S, "Analysis of PV-hydro isolated power systems," *2013 Annual IEEE India Conference (INDICON)*, pp. 1-6. 2013.
- [8] Hasmaini Mohamada,b, Hazlie Mokhlisa, Ab Halim Abu Bakara, Hew Wooi Ping, "A review on islanding operation and control for distribution network connected with small hydro power plant," *Renewable and Sustainable Energy Reviews*, vol.15, pp.3952-3962, August. 2011.
- [9] Khalilzadeh, E., Fotuhi-Firuzabad, M., Aminifar, F., Ghaedi, A., "Reliability Modeling of Run-of-the-River Power Plants in Power

- System Adequacy Studies," *Sustainable Energy, IEEE Transactions on*, vol. 5, No. 4, pp. 1949-3029, Oct. 2014.
- [10] S. Mandelli et al. "A small-hydro plant model for feasibility analysis of electrification projects in Rural Tanzania," in *Proc. IEEE Global Humanitarian Technol. Conf. (GHTC)*, 2013, pp. 11–16.
- [11] Kim J. Y., Jeon J. H., Kim S. K., Cho C. H., Park J. H., Kim H. M., and Nam K. Y., "Cooperative control strategy of energy storage system and microsources for stabilizing the microgrid during islanded operation," *IEEE Trans. Power Electron.*, Vol. 25, No. 12, pp. 3037-3048, December 2010.
- [12] Jong-Yul Kim; Seul-Ki Kim; Jin-Hong Jeon, "Coordinated state-of-charge control strategy for microgrid during islanded operation," *Power Electronics for Distributed Generation Systems (PEDG), 2012 3rd IEEE International Symposium on*, pp.133-139, June 2012.
- [13] Caldognetto, T., Tenti, P., Costabeber, A., Mattavelli, P., "Improving Microgrid Performance by Cooperative Control of Distributed Energy Sources," *IEEE Transactions on Industry Applications*, vol. 50, no. 6, pp. 3921 - 3930, Nov. 2014.
- [14] Guerrero, J.M.; Chandorkar, M.; Lee, T.; Loh, P.C., "Advanced Control Architectures for Intelligent Microgrids—Part I: Decentralized and Hierarchical Control," *Industrial Electronics, IEEE Transactions on*, vol.60, no.4, pp.1254-1262, April 2013.
- [15] Savaghebi, M.; Jalilian, A.; Vasquez, J.C.; Guerrero, J.M., "Secondary Control for Voltage Quality Enhancement in Microgrids," *Smart Grid, IEEE Transactions on*, vol.3, no.4, pp.1893-1902, Dec. 2012.
- [16] J. C. Vasquez, J. M. Guerrero, J. Miret, M. Castilla, L. G. de Vicuña, "Hierarchical Control of Intelligent Microgrids," *IEEE Industrial Electronics Magazine*, vol.4, no.4, pp.23-29, Dec. 2010.
- [17] J. M. Guerrero, J. C. Vasquez, J. Matas, M. Castilla, de Vicuña, L.G., Castilla, M., "Hierarchical control of droop-controlled AC and DC microgrids—A general approach toward standardization," *IEEE Trans. Ind. Electron.*, vol. 58, no. 1, pp. 158–172, Jan. 2011.
- [18] Y. A. R. I.Mohamed and A. A. Radwan, "Hierarchical control system for robust microgrid operation and seamless mode transfer in active distribution systems," *IEEE Trans. Smart Grid*, vol. 2, no. 2, pp. 352–362, Jun. 2011.
- [19] Thale, S., Wandhare, R.G., Agarwal, V, "A Novel Reconfigurable Microgrid Architecture with Renewable Energy Sources and Storage," *IEEE Transactions on Industry Applications*, to be published.
- [20] Yunwei Li, Vilathgamuwa, D.M., Poh Chiang Loh, "Design, Analysis, and Real-Time Testing of a Controller for Multibus Microgrid System," *IEEE Transactions on Power Electronics*, vol. 19, no. 5, pp. 1195–1204, Sept. 2004.
- [21] Guerrero, J.M., Garcia De Vicuna, L., Matas, J., Castilla, M., Miret, J., "Output Impedance Design of Parallel-Connected UPS Inverters With Wireless Load-Sharing Control," *IEEE Transactions on Industrial Electronics*, vol. 52, no. 4, 1126-1135, Aug. 2005
- [22] S. J. Chiang, C. Y. Yen, and K. T. Chang, "A multimodule parallelable series-connected PWM voltage regulator," *IEEE Trans. Ind. Electron.*, vol. 48, no. 3, pp. 506–516, Jun. 2001.
- [23] Engler, A.; Soltanis, N., "Droop control in LV-grids," *Future Power Systems, 2005 International Conference on*, vol., no., pp.6, 18-18 Nov. 2005
- [24] Guerrero, J.M.; Matas, J.; Luis Garcia de Vicuna; Castilla, M.; Miret, J., "Decentralized Control for Parallel Operation of Distributed Generation Inverters Using Resistive Output Impedance," *Industrial Electronics, IEEE Transactions on*, vol.54, no.2, pp.994-1004, April Apr. 2007
- [25] Chia-Tse Lee, Ruei-Pei Jiang, Po-Tai Cheng, "A Grid Synchronization Method for Droop-Controlled Distributed Energy Resource Converters," *IEEE Transactions on Industry Applications*, vol. 49, no. 2, pp. 954-962, Mar. 2013.
- [26] Savaghebi, M.; Vasquez, J.C.; Jalilian, A.; Guerrero, J.M.; Tzung-Lin Lee, "Selective harmonic virtual impedance for voltage source inverters with LCL filter in microgrids," *Energy Conversion Congress and Exposition (ECCE), 2012 IEEE*, vol., no., pp.1960-1965, 15-20 Sept. 2012
- [27] Prabha Kundur, *Power System Stability and Control*, 1st ed., New York: McGraw-Hill, 1993, pp. 315-1022.
- [28] P.K Olulope, K.A Folly, Ganesh K. Venayagamoorthy, "Modeling and simulation of hybrid distributed generation and its impact on transient stability of power system," *Industrial Technology (ICIT), 2013 IEEE International Conference on*, pp.1757-1762, Feb. 2013.
- [29] J. H. Zhou, P. L. X. H. Ge, X. S. Zhang, X. Q. Gao, Y. Liu, "Stability Simulation of a MW-Scale PV-Small Hydro Autonomous Hybrid System," *Power and Energy Society General Meeting (PES), 2013 IEEE*, pp.1-5, July 2013.
- [30] F. Katiraei, M.R. Irvani, P.W. Lehn, "Small-signal dynamic model of a micro-grid including conventional and electronically interfaced distributed resources," *IET Gener. Transm. Distrib.*, vol. 1, no. 3, pp. 369–378, 2007
- [31] Hongqing Fang, Long Chen, Dlakavu, N., Zuyi Shen, "Basic Modeling and Simulation Tool for Analysis of Hydraulic Transients in Hydroelectric Power Plants," *Energy Conversion, IEEE Transactions on*, vol. 23, no. 3, pp. 834 - 841, Sept. 2008.
- [32] NagarajuPogaku, Milan Prodanovic', and Timothy C. Green, "Modeling, Analysis and Testing of Autonomous Operation of an Inverter-Based Microgrid," *IEEE Trans Power Electronics*, vol. 22, no. 2, MAR 2007.
- [33] Kroutikova, N., Hernandez-Aramburo, C.A., Green, T.C, "State-space model of grid-connected inverters under current control mode," *Electric Power Applications, IET*, vol. 1, no. 3, pp. 329–338, May. 2007.
- [34] Alireza Kahrobaeian, Yasser Abdel-Rady I. Mohamed, "Analysis and Mitigation of Low-Frequency Instabilities in Autonomous Medium-Voltage Converter-Based Microgrids With Dynamic Loads," *IEEE Trans. Industrial Electronics*, vol. 61, no. 4, pp.1643-1658, April. 2014
- [35] Coelho, E.A.A.; Cortizo, P.C.; Garcia, P.F.D., "Small-signal stability for parallel-connected inverters in stand-alone AC supply systems," *Industry Applications, IEEE Transactions on*, vol.38, no.2, pp.533-542, Mar/Apr. 2002
- [36] Souza, O.H., Jr., Barbieri, N., Santos, A.H.M., "Study of hydraulic transients in hydropower plants through simulation of nonlinear model of penstock and hydraulic turbine model," *IEEE Transactions on Power Systems*, vol. 14, no. 4, pp. 1269 – 1272, Nov. 1999.
- [37] Thorne, D.H., Hill, E.F., "Field Testing and Simulation of Hydraulic Turbine Governor Performance," *Power Apparatus and Systems, IEEE Transactions on*, vol.93, no.4, pp.1183-1191, July 1974.
- [38] Juan C. Vasquez, Josep M. Guerrero, Mehdi Savaghebi, Joaquin Eloy-Garcia, Remus Teodorescu, "Modeling, Analysis, and Design of Stationary-Reference-Frame Droop-Controlled Parallel Three-Phase Voltage Source Inverters," *Industrial Electronics, IEEE Transactions on*, vol. 60, no. 4, pp. 1271 – 1280, April. 2013.
- [39] Shafiee, Q., Guerrero, J.M., Vasquez, J.C., "Distributed Secondary Control for Islanded Microgrids—A Novel Approach," *Power Electronics, IEEE Transactions on*, vol. 29, No. 2, pp. 1018 – 1031, Feb. 2014.
- [40] Shafiee, Q., Stefanovic, C., Dragicevic, T., Popovski, P., Vasquez, J.C., Guerrero, J.M., "Robust Networked Control Scheme for Distributed Secondary Control of Islanded Microgrids," *Industrial Electronics, IEEE Transactions on*, vol. 61, no. 10, pp. 5363 – 5374, Oct. 2014.
- [41] Lexuan Meng, Fen Tang, Mehdi Savaghebi, Juan C. Vasquez, Josep M. Guerrero, "Tertiary Control of Voltage Unbalance Compensation for Optimal Power Quality in Islanded Microgrids," *IEEE Trans. Energy Conv.*, vol. 29, no. 4, pp. 802 - 815, Dec. 2014.
- [42] *IEEE Guide for the Application of Turbine Governing Systems for Hydroelectric Generating Units*, IEEE Std 1207™-2011, June, 2011.
- [43] Hagihara, S., Yokota, H., Goda, K., Isobe, K., "Stability of a Hydraulic Turbine Generating Unit Controlled by P.I.D. Governor," *Power Apparatus and Systems, IEEE Transactions on*, vol. PAS-98, no. 6, pp. 2294 - 2298, Nov. 1979.
- [44] E. Ghahremani, M. Karrari, O.P. Malik, "Synchronous generator third-order model parameter estimation using online experimental data," *IET Gener. Transm. Distrib.*, vol. 2, no. 5, pp. 708 - 719, April, 2008.
- [45] Alizadeh, G., Ghiasi, A.R., Javadi, "A.Nonlinear H[∞] Control of a Third-Order Synchronous Generator Model," *Ultra Modern Telecommunications and Control Systems and Workshops (ICUMT), 2012 4th International Congress on*, pp. 455-461, 2012.
- [46] *IEEE Recommended Practice for Excitation System Models for Power System Stability Studies*, IEEE Std 421.5-1992, March, 1992.



Yajuan Guan (S'14) received the B.S. degree and M.S. degree in Electrical Engineering from the Yanshan University, Qinhuangdao, Hebei, China, in 2007 and 2010 respectively. From 2010 to 2012, she was an Assistant Professor in Institute of Electrical Engineering (IEE), Chinese Academy of Sciences (CAS). Since 2013, she has been a Lecturer in IEE; CAS. She is currently working toward her Ph.D. degree at the Department of Energy Technology, Aalborg University, Denmark, as part of the Denmark Microgrids Research Programme (www.microgrids.et.aau.dk).

Her research interests include microgrids, distributed generation systems, power converter for renewable energy generation systems, and ancillary services for microgrids.



Juan C. Vasquez (M'12-SM'14) received the B.S. degree in electronics engineering from the Autonomous University of Manizales, Manizales, Colombia, and the Ph.D. degree in automatic control, robotics, and computer vision from the Technical University of Catalonia, Barcelona, Spain, in 2004 and 2009, respectively. He was with the Autonomous University of Manizales, where he taught courses on digital circuits, servo systems, and flexible manufacturing systems. He was also with the Technical University of Catalonia, as a Post-Doctoral Assistant, teaching courses based on renewable energy systems. In 2011, he was Assistant Professor in microgrids and currently he is working as an Associate Professor at the Department of Energy Technology, Aalborg University, Denmark. Dr. Vasquez is the co-responsible of the Research Program in Microgrids. From Feb. 2015 to April. 2015 he was a Visiting Scholar at the Center of Power Electronics Systems (CPES) at Virginia Tech.

His current research interests include operation, power management, hierarchical control, optimization and power quality applied to distributed generation and ac/dc microgrids. Dr. Vasquez is currently a member of the IEC System Evaluation Group SEG4 on LVDC Distribution and Safety for use in Developed and Developing Economies and the Renewable Energy Systems Technical Committee TC-RES in IEEE Industrial Electronics Society.



Josep M. Guerrero (S'01-M'04-SM'08-FM'15) received the B.S. degree in telecommunications engineering, the M.S. degree in electronics engineering, and the Ph.D. degree in power electronics from the Technical University of Catalonia, Barcelona, in 1997, 2000 and 2003, respectively. Since 2011, he has been a Full Professor with the Department of Energy Technology, Aalborg University, Denmark, where he is responsible for the Microgrid Research Program. From 2012 he is a guest Professor at the Chinese Academy of

Science and the Nanjing University of Aeronautics and Astronautics; from 2014 he is chair Professor in Shandong University; and from 2015 he is a distinguished guest Professor in Hunan University.

His research interests is oriented to different microgrid aspects, including power electronics, distributed energy-storage systems, hierarchical and cooperative control, energy management systems, and optimization of microgrids and islanded minigrids. Prof. Guerrero is an Associate Editor for the IEEE TRANSACTIONS ON POWER ELECTRONICS, the IEEE TRANSACTIONS ON INDUSTRIAL ELECTRONICS, and the IEEE Industrial Electronics Magazine, and an Editor for the IEEE TRANSACTIONS ON SMART GRID and IEEE TRANSACTIONS ON ENERGY CONVERSION. He has been Guest Editor of the IEEE TRANSACTIONS ON POWER ELECTRONICS Special Issues: Power

Electronics for Wind Energy Conversion and Power Electronics for Microgrids; the IEEE TRANSACTIONS ON INDUSTRIAL ELECTRONICS Special Sections: Uninterruptible Power Supplies systems, Renewable Energy Systems, Distributed Generation and Microgrids, and Industrial Applications and Implementation Issues of the Kalman Filter; and the IEEE TRANSACTIONS ON SMART GRID Special Issue on Smart DC Distribution Systems. He was the chair of the Renewable Energy Systems Technical Committee of the IEEE Industrial Electronics Society. In 2014 he was awarded by Thomson Reuters as Highly Cited Researcher, and in 2015 he was elevated as IEEE Fellow for his contributions on "distributed power systems and microgrids."



Yibo Wang was born in 1977. He received the Ph.D degree from the Institute of Electrical Engineering (IEE), Chinese Academy of Sciences (CAS) in 2009. Currently, he is a professor in IEE, CAS. His research fields focus on renewable energy system and micro-grid, and his main research interests include system analysis and design, grid integration, power conversion, control and protection of renewable energy systems and microgrids.



Wei Feng received the B.Sc. and M.Sc. degrees in Automation from the Beijing Jiaotong University, Beijing, China, in 2006 and 2008, respectively. He received the Ph.D. degree in power electronics and motor drive from the Institute of Electrical Engineering, Chinese Academy of Sciences, Beijing, in 2014. He is currently a Post-Doc in Tsinghua University, China. His research interests include control of paralleled inverters for renewable generation systems, power quality improvement and energy management system for microgrids.